



Space Weather

RESEARCH ARTICLE

10.1029/2018SW001875

Special Section:

Low Earth Orbit Satellite Drag: Science and Operational Impact

Key Points:

- Calibration of quasi-physical reduced-order model of the thermosphere via data assimilation with a Kalman Filter
- Estimation of the model parameters rather than the driver ($F_{10.7}$) for a calibrated model
- Global field calibration using CHAMP-derived density estimates along its orbit

Correspondence to:

P. M. Mehta,
piyushmukeshmehta@gmail.com

Citation:

Mehta, P. M., & Linares, R. (2018). A new transformative framework for data assimilation and calibration of physical ionosphere-thermosphere models. *Space Weather*, 16, 1086–1100. <https://doi.org/10.1029/2018SW001875>

Received 30 MAR 2018

Accepted 14 JUN 2018

Accepted article online 21 JUN 2018

Published online 20 AUG 2018

A New Transformative Framework for Data Assimilation and Calibration of Physical Ionosphere-Thermosphere Models

Piyush M. Mehta¹  and Richard Linares²

¹Department of Mechanical and Aerospace Engineering, Statler College of Engineering and Mineral Resources, West Virginia University, Morgantown, WV, USA, ²Department of Aeronautics and Astronautics, Massachusetts Institute of Technology, Cambridge, MA, USA

Abstract Accurate specification and prediction of the ionosphere-thermosphere environment, driven by external forcing, is crucial to the space community. In this work, we present a new transformative framework for data assimilation and calibration of the physical ionosphere-thermosphere models. The framework has two main components: (i) the development of a quasi-physical dynamic reduced-order model (ROM) that uses a linear approximation of the underlying dynamics and effect of the drivers, and (ii) data assimilation and calibration of the ROM through estimation of the ROM coefficients that represent the model parameters. A reduced-order surrogate for thermospheric mass density from the Thermosphere-Ionosphere-Electrodynamics General Circulation Model (TIE-GCM) was developed in previous work. This work concentrates on the second component of the framework—data assimilation and calibration of the TIE-GCM ROM. The new framework has two major advantages: (i) a dynamic ROM that combines the speed of empirical models for real-time capabilities with the predictive capabilities of physical models, which has the potential to facilitate improved uncertainty quantification using large ensembles, and (ii) estimation of model parameters rather than the driver(s)/input(s), which allows calibration of the model, thus avoiding degradation of model performance in the absence of continuous data. We demonstrate and validate the framework using simulated and real measurement scenarios. The simulated case uses Mass Spectrometer and Incoherent Scatter model output as measurements, while the real data case uses accelerometer-derived density estimates from CHALLENGING Minisatellite Payload and Gravity Field and Steady-State Ocean Circulation Explorer. The framework is a first of its kind, simple yet robust and accurate method with high potential for providing real-time operational updates to the state of the upper atmosphere in the context of drag modeling for space situational awareness and space traffic management.

1. Introduction

The upper atmosphere, comprising the ionosphere-thermosphere (IT), is a highly dynamic environment that readily undergoes variations that can be significant under certain conditions. Accurate modeling and prediction of the IT variations, caused by space weather events (SWEs), are crucial for safeguarding the space assets that serve various communities. Ionospheric enhancements caused by SWEs can hinder telecommunications while also affecting systems on-board the assets directly through surface charging and other phenomenon. Thermospheric mass density enhancements caused by SWEs have a direct and strong impact on the drag force acting on the space assets and other objects in low Earth orbit (LEO). Existing models for the thermosphere can be highly biased or erroneous, especially for forecasts, making drag the largest source of uncertainty in our ability to accurately predict the state of the objects in LEO. With the recent increase in space traffic (Radtke et al., 2017), predicting the state of the objects in LEO becomes critical for collision avoidance in the context of space situational awareness (SSA) and space traffic management (STM).

Empirical models of the thermosphere (Barlier et al., 1978; Berger et al., 1998; Bowman, Tobiska, Marcos, Huang, et al., 2008; Bowman, Tobiska, Marcos, & Valladares, 2008; Bruinsma et al., 2003, 2012, 2015; Hedin, 1983, 1987; Hedin et al., 1977; Jacchia, 1970; Picone et al., 2002), developed since early in the space age using sparse measurements, adopt a climatological approach to model the variations of the thermosphere. These models capture the behavior in an average sense using low-order, parameterized mathematical for-

mulations tuned to observations. A major advantage of the empirical models is that they are fast to evaluate, making them ideal for drag and SSA/STM applications. The current state of practice employed by the Joint Space Operations Center under the direction of the U.S. Air Force Space Command is an operational assimilative empirical model that makes dynamic adjustments based on recent measurements of the state of the thermosphere (Storz et al., 2005) but lacks in its ability for providing accurate forecasts.

The upper atmosphere is a large-scale nonlinear physical dynamical system with exogenous inputs, including from the Sun, which is its strongest driver. The first principles based physical models of the IT carry good potential for forecast; however, realizing that potential requires significant advances in data assimilation methods. Data assimilation is the process of fusing observational data into numerical models to reduce uncertainty in the model forecast. Data assimilation is required for physical models due to the imperfect nature of the dynamics embedded in them that allows empirical models to consistently outperform them in terms of accuracy (Shim et al., 2014).

Over the last decade or two, significant advances have been made in development of data assimilation methods with IT models for neutral density and drag applications. The said methods have been successful in achieving better agreement between the measurements and model but lack in consistently providing nowcasts and forecasts that can compete with current state of practice (Sutton, 2018)—the High Accuracy Satellite Drag Model (Storz et al., 2005). Most methods for data assimilation with physical models either achieve this by estimating the state, the driver(s), or some combination of the two (Codrescu et al., 2004, 2018; Fuller-Rowell et al., 2004; Godinez et al., 2015; Matsuo & Knipp, 2013; Matsuo et al., 2012, 2013; Minter et al., 2004; Morozov et al., 2013; Murray et al., 2015; Sutton, 2018). The state can either be the parameter of interest (model output) or model parameters that relate the output to the input. Because physical models solve the discretized fluid equations over a volumetric grid, the full state can be rather large in size (over a million estimated parameters). Traditional data assimilation methods, based on the Ensemble Kalman filter, estimate both the input drivers as well internal state of the model because the variational timescales in the thermosphere can cause a lag in the filter. The large state vector combined with the large number of ensembles needed to obtain statistically significant results makes the approach computationally expensive. Recent approach by Sutton (2018) uses predefined model variation runs in lieu of large ensembles combined with an iterative approach to prevent filter lag in estimation of the dominant drivers ($F_{10.7}$ and K_p) for a self-consistent calibration of the model. The approach, however, remains computationally expensive requiring dedicated parallel resources for real-time application, but more importantly, the estimation can result in physically unrealistic values for the driver(s) as previous methods that estimate them. In addition, the method of estimating driver(s) is not robust against a break in continuous data stream as the model forecast falls back to the original evolution of the model and is currently an open question in the community (H. Godinez, private communication, February 12, 2018). Moreover, with the final goal of accurate uncertainty quantification for the computation of collision probabilities, the current methods lie somewhere between highly computationally expensive to intractable.

This paper demonstrates a new two-part transformative framework for data assimilation and calibration of physical IT models with the potential for providing accurate density forecasts and uncertainty quantification. The framework has two main components: (i) development of a quasi-physical reduced-order model (ROM) and (ii) calibration of the ROM through data assimilation. Previous work presented the development of a new method, Hermitian Space-Dynamic Mode Decomposition with control (HS-DMDc), towards achieving model order reduction for large-scale dynamical IT models (Mehta, Linares, & Sutton, 2018). The new method carries the same motivation and goals as previous work using Proper Orthogonal Decomposition (POD) or Empirical Orthogonal Functions (EOFs; e.g., Matsuo et al., 2012; Mehta & Linares, 2017) but uses a dynamic systems formulation that inherently facilitates prediction. The ROM provides a linearized representation of the underlying model dynamics. In this paper, we demonstrate a simple yet robust and effective approach for estimating and calibrating the state of the thermosphere using the ROM with data assimilation. The approach uses a standard Kalman filter to estimate a reduced state that represents the model parameters rather than the driver(s), which avoids degradation of the model performance in the absence of measurement data. In addition, the ROM can provide a 24-hr forecast in a fraction of a second on a standard desktop platform. In essence, the framework combines the best of both empirical (low-cost) and physical (predictive capabilities) models and can also facilitate accurate uncertainty quantification with large ensemble simulations (subject of future work).

The paper is organized as follows: section 2 describes the process of developing a quasi-physical dynamic ROM using discrete time simulation output from physical IT systems. Section 3 describes the conversion of the ROM between discrete and continuous time, essential for assimilating data using a Kalman filter in the new framework. Section 4 describes the accelerometer-derived density measurements used in this work for data assimilation. Section 5 gives a brief overview of the very popular Kalman filter including the Bayesian Optimization (BO) approach used to optimize the filter in this work. Section 6 answers the question of observability, and section 7 presents and discusses the results of data assimilation. Finally, section 8 concludes the paper.

2. Model Order Reduction

The main idea behind reduced-order modeling is to reduce the complexity of a physical model by reducing the state space dimension or degrees of freedom of the system. POD (Lumley, 1967) or EOF is the most commonly used approach for model order reduction; however, one of its major limitation is that the formulation does not allow prediction. POD reconstructs the state (\mathbf{x}) using a small number (r) of spatial structures or modes (ϕ) combined with the corresponding time-dependent coefficients (c_i) as given below:

$$\tilde{\mathbf{x}}(\mathbf{s}, t) = \mathbf{x}(\mathbf{s}, t) - \bar{\mathbf{x}}(\mathbf{s}) \approx \sum_{i=1}^r c_i(t) \phi_i(\mathbf{s}) \quad (1)$$

In the equation above, the decomposition is performed after taking away the mean; therefore, the first r modes capture a significant fraction of the variance. If the decomposition is performed without taking away the mean, as in the present paper, the first r modes capture a large fraction of the energy with the first mode containing a strong mean component. For more details the reader is directed to Mehta and Linares (2017) and Mehta, Linares, and Sutton (2018). The POD method can provide insights into the underlying dynamics of the system through the spatial structures or modes and the temporal variation of the corresponding coefficients but cannot model its evolution for prediction. Several studies have attempted to overcome this limitation using surrogate or parameterized models (e.g., Mehta & Linares, 2017); however, the upper atmosphere is a physical dynamical system and should be appropriately modeled as such.

Dynamic Model Decomposition (DMD), developed by Schmid (2010), uses a dynamic systems formulation that inherently enables prediction. The method derives an approximation for the dynamic matrix, \mathbf{A} , of a best fit linear system that can be used for prediction in discrete time as

$$\mathbf{x}_{k+1} = \mathbf{A}\mathbf{x}_k \quad (2)$$

Proctor et al. (2016) extended DMD for application to systems with exogenous inputs

$$\mathbf{x}_{k+1} = \mathbf{A}\mathbf{x}_k + \mathbf{B}\mathbf{u}_k \quad (3)$$

where \mathbf{B} is the input matrix. Because computing and storing the dynamic and input matrices for a large state ($\mathbf{x} \gg 1$) can be intractable, a reduced-order representation of the system is achieved through a similarity transform that projects the state, and the dynamic and input matrices onto a reduced space given by the POD modes as discussed in detail later in the section.

Mehta, Linares, and Sutton (2018) used the Hermitian Space to extend application to large-scale systems such as the upper atmosphere; they call the method HS-DMDc. They developed a ROM using simulation output from National Center for Atmospheric Research's TIE-GCM (Thermosphere-Ionosphere-Electrodynamics General Circulation Model; Qian et al., 2014) spanning over a full solar cycle (12 years). The reader is referred to Mehta, Linares, and Sutton (2018) for detailed information on ROM for IT models. In this paper, we provide basic knowledge relevant to the process of data assimilation.

Large-scale physical models of the IT solve discretized fluid equations over a grid on interest. In discrete time, the evolution of a linear dynamical system can be given as in equation (3), where $\mathbf{A} \in \mathbb{R}^{n \times n}$ is the dynamic matrix and $\mathbf{B} \in \mathbb{R}^{n \times p}$ is the input matrix in discrete time, $\mathbf{x} \in \mathbb{R}^{n \times 1}$ is the full state, $\mathbf{u} \in \mathbb{R}^{p \times 1}$ is the input, and k is the time index. HS-DMDc uses time-resolved snapshots, \mathbf{x}_k , from a physical system (in this case TIE-GCM simulation output) to extract the best fit estimate for \mathbf{A} and \mathbf{B} . Modeling the nonlinear dynamics with a reduced form will be the subject of future work. In order for the derived model to be applicable across the full range of input conditions, the ROM was derived using 12 years of TIE-GCM simulations spanning a full solar cycle. Because 12 years, worth of simulation output or snapshots results in a large data set, the innovation behind

HS-DMDc is to reduce the problem to the Hermitian Space (computing the inverse of a matrix $\mathbf{X} \in \mathbb{R}^{n \times (m-1)}$, m being the number of snapshots, is reduced to taking an inverse of $\mathbf{X}\mathbf{X}^T \in \mathbb{R}^{n \times n}$).

HS-DMDc uses snapshot matrices that are a collection of the time-resolved output from TIE-GCM to estimate the dynamic and input matrices. The three-dimensional grid outputs over time are unfolded into column vectors and stacked together. The input matrix is an assimilation of the inputs to the system. In this case, the inputs used are the solar activity proxy ($F_{10.7}$), geomagnetic proxy (K_p), universal time (UT) and day of the year.

$$\mathbf{X}_1 = \begin{bmatrix} | & | & \cdots & | \\ \mathbf{x}_1 & \mathbf{x}_2 & \cdots & \mathbf{x}_{m-1} \\ | & | & \cdots & | \end{bmatrix} \quad \mathbf{X}_2 = \begin{bmatrix} | & | & \cdots & | \\ \mathbf{x}_2 & \mathbf{x}_3 & \cdots & \mathbf{x}_m \\ | & | & \cdots & | \end{bmatrix} \quad \mathbf{Y} = \begin{bmatrix} | & | & \cdots & | \\ \mathbf{u}_1 & \mathbf{u}_2 & \cdots & \mathbf{u}_{m-1} \\ | & | & \cdots & | \end{bmatrix} \quad (4)$$

The snapshot and input matrices are related by Equation (3) such that

$$\mathbf{X}_2 = \mathbf{A}\mathbf{X}_1 + \mathbf{B}\mathbf{Y} \quad (5)$$

The goal now is to estimate \mathbf{A} and \mathbf{B} . In order to achieve this, the above equation is modified such that

$$\mathbf{X}_2 = \mathbf{Z}\Psi \quad (6)$$

where \mathbf{Z} and Ψ are the augmented operator and data matrices, respectively.

$$\mathbf{Z} \triangleq [\mathbf{A} \ \mathbf{B}] \quad \text{and} \quad \Psi \triangleq \begin{bmatrix} \mathbf{X}_1 \\ \mathbf{Y} \end{bmatrix} \quad (7)$$

The estimate for \mathbf{Z} , and hence \mathbf{A} and \mathbf{B} , is achieved with a Moore-Penrose pseudoinverse of Ψ such that $\mathbf{Z} = \mathbf{X}_2\Psi^\dagger$.

Because the state size, n , can also be very large making computation and storage of the dynamic and input matrices intractable, a reduced state is used to model the evolution of the dynamical system.

$$\mathbf{z}_{k+1} = \mathbf{A}_r\mathbf{z}_k + \mathbf{B}_r\mathbf{u}_k + \mathbf{w}_k \quad (8)$$

where $\mathbf{A}_r \in \mathbb{R}^{r \times r}$ is the reduced dynamic matrix and $\mathbf{B}_r \in \mathbb{R}^{r \times p}$ is the reduced input matrix in discrete time, $\mathbf{z} \in \mathbb{R}^{r \times 1}$ is the reduced state, and \mathbf{w}_k is the process noise that accounts for the unmodeled effects and the ROM truncation error. The state reduction is achieved using a similarity transform $\mathbf{z}_k = \mathbf{U}_r^\dagger \mathbf{x}_k = \mathbf{U}_r^T \mathbf{x}_k$, where \mathbf{U}_r are the first r POD modes. The steps involved in HS-DMDc are summarized below. The data assimilation process presented in this work will estimate the reduced state, \mathbf{z} , that represents the coefficients of the POD modes and can be thought of as model parameters that relate the model input(s) to the output(s). It can also provide insights into the model dynamics and will be explored in future work.

Algorithm 1 Hermitian Space-Dynamic Mode Decomposition With control

1. Construct the data matrices \mathbf{X}_1 , \mathbf{X}_2 , \mathbf{Y} , and Ψ .
2. Compute the pseudoinverse of Ψ using an economy eigendecomposition (E-ED) in the Hermitian Space. The choice of \hat{r} depends on several factors.

$$\Psi\Psi^T = \hat{\mathbf{U}}_r \hat{\mathbf{\Xi}}_r \hat{\mathbf{U}}_r^T \quad (9)$$

$$\implies \Psi^\dagger = \Psi^T(\Psi\Psi^T)^{-1} = \Psi^T(\hat{\mathbf{U}}_r \hat{\mathbf{\Xi}}_r \hat{\mathbf{U}}_r^T)^{-1} = \Psi^T \hat{\mathbf{U}}_r \hat{\mathbf{\Xi}}_r^{-1} \hat{\mathbf{U}}_r^T \quad (10)$$

3. Perform a second E-ED in the Hermitian space to derive the POD modes (\mathbf{U}_r) for reduced-order projection. Choose the truncation value r such that $\hat{r} > r$.

$$\mathbf{X}_1\mathbf{X}_1^T = \mathbf{U}_r \mathbf{\Xi}_r \mathbf{U}_r^T \quad (11)$$

4. Compute the reduced-order dynamic and input matrices

$$\tilde{\mathbf{A}} = \mathbf{U}_r^T \mathbf{X}_2 \Psi \hat{\mathbf{U}}_r \hat{\mathbf{\Xi}}_r^{-1} \hat{\mathbf{U}}_{r,1}^T \mathbf{U}_r \quad (12)$$

$$\tilde{\mathbf{B}} = \mathbf{U}_r^T \mathbf{X}_2 \Psi \hat{\mathbf{U}}_r \hat{\mathbf{\Xi}}_r^{-1} \hat{\mathbf{U}}_{r,2}^T \quad (13)$$

where $\hat{\mathbf{U}}_r^T = [\hat{\mathbf{U}}_{r,1}^T \ \hat{\mathbf{U}}_{r,2}^T]$ with $\hat{\mathbf{U}}_{r,1} \in \mathbb{R}^{n \times r}$ and $\hat{\mathbf{U}}_{r,2} \in \mathbb{R}^{p \times r}$

3. Discrete to Continuous Time

The new framework uses a sequential (Kalman) filter for data assimilation that requires propagating the state to the next measurement time, which most likely will not be uniformly distributed and/or with a snapshot resolution used to derive the dynamic and input matrices for the ROM. Therefore, the dynamic and input matrices need to be first converted to continuous time and then back to time for next measurement, t_k . This can be achieved using the following relation (DeCarlo, 1989):

$$\begin{bmatrix} \mathbf{A}_c & \mathbf{B}_c \\ \mathbf{0} & \mathbf{0} \end{bmatrix} = \log \left(\begin{bmatrix} \mathbf{A}_d & \mathbf{B}_d \\ \mathbf{0} & \mathbf{I} \end{bmatrix} \right) / T \quad (14)$$

where $[\mathbf{A}_c, \mathbf{A}_d]$ are the dynamic matrices and $[\mathbf{B}_c, \mathbf{B}_d]$ are the input matrices in continuous and discrete time, respectively, and T is the sample time (snapshot resolution when converting from discrete to continuous time and the time to next measurement, t_k , when converting back from continuous to discrete time). This represents another major advantage of the new framework where the time step of model evolution can be readily adjusted.

4. Measurements

Because the TIE-GCM ROM used for this demonstration is restricted to altitudes between 100 and 450 km for reasons discussed in Mehta, Linares, and Sutton (2018), we cannot use the pair of CHAMP (CHALLENGING Minisatellite Payload; Reigber et al., 2002) and GRACE (Gravity Recovery and Climate Experiment; Tapley et al., 2004) accelerometer-derived high-accuracy measurements of thermospheric mass density. CHAMP and GRACE accelerometer-derived mass density estimates have been the workhorse for a lot of work that has been done in the area; therefore, we use CHAMP-derived measurements in conjunction with density estimates derived from accelerometer measurements on board the GOCE (Gravity Field and Steady-State Ocean Circulation Explorer) satellite (Drinkwater et al., 2003). We use the state-of-the-art CHAMP density estimates from Mehta et al. (2017) and the latest GOCE data set from Doornbos et al. (2014). The simulated case uses the Naval Research Laboratory's MSIS (Mass Spectrometer and Incoherent Scatter) model (Picone et al., 2002) output along CHAMP and GOCE satellites as measurements.

Because the existing models, empirical and physical, have the largest bias/difference with accelerometer-derived densities at solar minimum and geomagnetically active conditions (Mehta et al., 2017), we choose a representative day (of the year: 320) in November 2009 to demonstrate the new framework. This period is also chosen because GOCE was launched in March 2009 and data for both CHAMP and GOCE are available. CHAMP is in a nearly polar orbit at close to 320-km altitude on the day chosen for assimilation. GOCE is in a Sun-synchronous orbit close to 250 km in altitude. Figure 1 shows the orbital elements for the two satellites on the day of assimilation. The two orbits are significantly different on the day of the assimilation, which validates the performance of the assimilation on a global scale. We choose a day with low geomagnetic activity as the current version of the TIE-GCM ROM is not applicable during active storm periods because of the linear approximation. This limitation is discussed in detail in Mehta et al. (2017). Demonstration for active time periods will be subject of future work. Both CHAMP- and GOCE-derived density estimates have a time resolution of 10 s. As with most of the previous work with data assimilation of IT models, we perform intercalibration of the two data sets with respect to TIE-GCM. We divide the CHAMP data with a daily factor of 1.35. For the simulated case, the MSIS CHAMP densities are scaled by a daily factor of 1.21. Also, as in previous work by the authors, development of the TIE-GCM ROM and assimilation of CHAMP densities is performed in the log scale (Emmert & Picone, 2010).

5. Kalman Filter

The sequential (Kalman) Filter, henceforth referred to in this work as KF, has been the workhorse for state estimation and prediction using discrete time linear systems since its inception at the beginning of the space age (Kalman, 1960). The KF is a linear optimal state estimation method that uses statistical (Bayesian) inference based on the Bayes' theorem (Bayes, 1763). Since the KF is one of the most commonly used tools in estimation theory, we will only provide a basic description with equations. There is a significant amount of literature available to the reader on Bayes' theorem, Bayesian inference, and KF should they be interested.

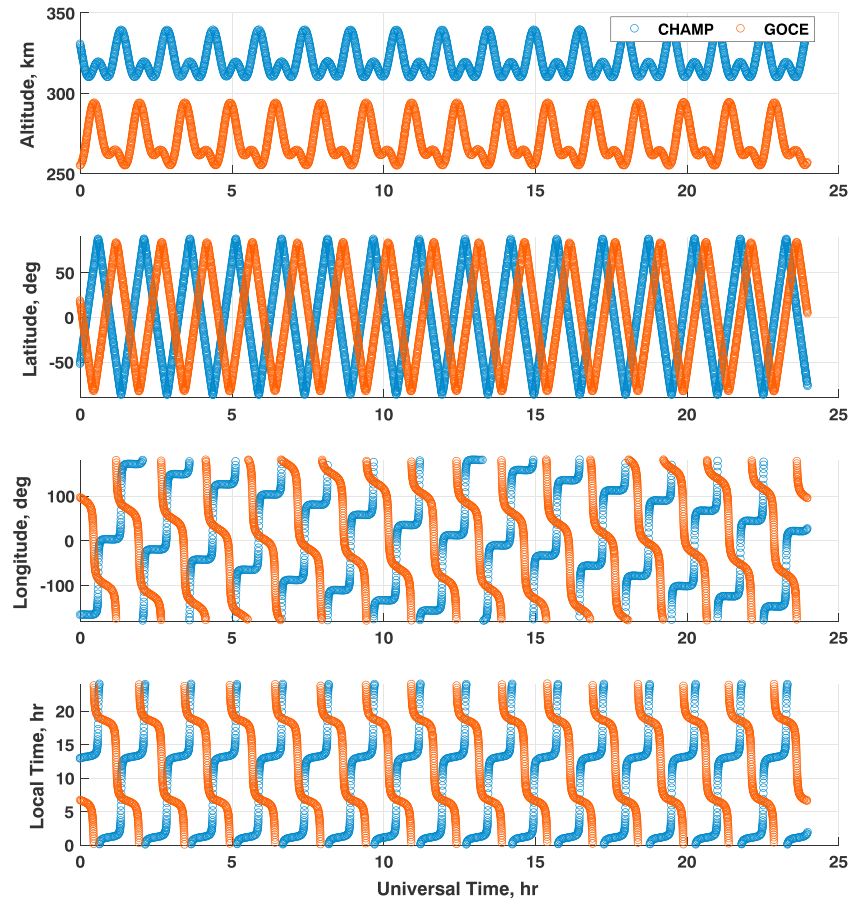


Figure 1. CHALLENGING Minisatellite Payload (CHAMP) and Gravity Field and Steady-State Ocean Circulation Explorer (GOCE) orbital elements on day 320 of year 2009.

The KF has two major steps: (i) time update and (ii) measurement update, as outlined in the algorithm below. The time update projects the current state and covariance estimate forward through the model to the time of next measurement. The projected state (\mathbf{x}_k^-) and covariance (\mathbf{P}_k^-), signified by the negative superscript, represent the a priori knowledge about the state of the system. The process noise (\mathbf{Q}) in equation (17) accounts for the imperfect model dynamics. The a priori covariance, the measurement variance (\mathbf{R}_k), and the observation matrix (\mathbf{H}_k) are combined to compute the Kalman Gain (\mathbf{K}_k) as given in equation (18). We generate a Monte Carlo estimate for \mathbf{R}_k in the log scale based on the uncertainties associated with the measurements (ρ , mass density) by sampling the Gaussian 100 times and recomputing the variance using the samples such that $\mathbf{R}_k \approx \text{Var} [\log(\rho_k + \Delta\rho_k * \text{randn}(100))]$. The observation matrix $\mathbf{H}_k^T \in \mathbb{R}^{r \times 1}$, which relates the measurements ($\tilde{\mathbf{y}}_k$) to the state (\mathbf{z}_k) by mapping it onto the measurement space, is in this case a vector made up of the interpolated values at the measurement location of the first r POD modes such that $\tilde{\mathbf{y}}_k = \mathbf{H}_k \mathbf{z}_k + \mathbf{v}_k$, where \mathbf{v}_k is the measurement error. In simple terms, the Kalman Gain reflects the weights or confidence for the a priori estimate against the measurement. The Kalman Gain is then used to update the a priori state and covariance estimate as given in equations (19) and (20). The updated state (\mathbf{x}_k^+) and covariance (\mathbf{P}_k^+), signified by the positive superscript, represent the posteriori knowledge about the state of the system achieved after data assimilation. The posteriori estimates are fed back into steps 1 and 2 until all the measurements have been processed. In the absence of measurements, the state and covariance are propagated through the model until a measurement is available.

5.1. Bayesian Optimization

A well-known challenge when applying the Kalman filter is the lack of knowledge on the process noise statistics. This work uses the process noise model to account for unmodeled effects that are not captured by TIE-GCM and errors induced in the model reduction process. Tuning the Kalman filter includes estimating statistics for process and measurement noise. However, we assume that the measurement noise values

reported for the data set used are accurate. Therefore, we only tune the process noise covariance. In addition, we tune the initial covariance (\mathbf{P}_0) as it is usually difficult to produce a good estimate for it.

BO is a method for blackbox optimization of stochastic cost function (Mockus, 1975). We use BO because our cost is a complex function of the process noise (\mathbf{Q}) and stochastic due to the measurement noise (\mathbf{R}). We use the cost function for maximum likelihood estimation given as

$$\min_{\mathbf{q}} L(\tilde{\mathbf{y}}|\mathbf{q}) = \sum_{k=1}^N \log (\det (\mathbf{R}_k + \mathbf{H}_k \mathbf{P}_k^+ \mathbf{H}_k^T)) + (\hat{\mathbf{y}}_k - \tilde{\mathbf{y}}_k)^T (\mathbf{R}_k + \mathbf{H}_k \mathbf{P}_k^+ \mathbf{H}_k^T)^{-1} (\hat{\mathbf{y}}_k - \tilde{\mathbf{y}}_k) \quad (15)$$

where $\hat{\mathbf{y}}_k$ is the estimated density and $\mathbf{Q} = \text{diag}(\mathbf{q})$, $\mathbf{q} \in \mathbb{R}^{r \times 1}$. We use the *bayesopt* function built into MATLAB for current work. The range of optimizable process noise \mathbf{Q} is set at $[1e-6, 1e-1]$. Because we estimate the reduced state that represents the POD coefficients, the range of optimizable initial covariance \mathbf{P}_0 is set at $[1e1, 1e2]$. The number of iterations is set at the default of 30. The optimized process noise matrix \mathbf{Q}_0 and initial covariance matrix \mathbf{P}_0 are then used to initialize the KF.

Algorithm 2 Kalman Filter

Time Update

1. Project the initial state estimate forward in time

$$\mathbf{x}_{k+1}^- = \mathbf{A} \mathbf{x}_k + \mathbf{B} \mathbf{u}_k \quad (16)$$

2. Project the initial covariance estimate forward in time

$$\mathbf{P}_{k+1}^- = \mathbf{A} \mathbf{P}_k \mathbf{A}^T + \mathbf{Q} \quad (17)$$

Measurement Update

3. Compute the Kalman Gain

$$\mathbf{K}_{k+1} = \mathbf{P}_{k+1}^- \mathbf{H}_{k+1}^T (\mathbf{H}_{k+1} \mathbf{P}_{k+1}^- \mathbf{H}_{k+1}^T + \mathbf{R}_{k+1})^{-1} \quad (18)$$

4. Update the state estimate

$$\mathbf{x}_{k+1}^+ = \mathbf{x}_{k+1}^- + \mathbf{K}_{k+1} (\tilde{\mathbf{y}}_{k+1} - \mathbf{H}_{k+1} \mathbf{x}_{k+1}^-) \quad (19)$$

5. Update the covariance estimate

$$\mathbf{P}_{k+1}^+ = (\mathbf{I} - \mathbf{K}_{k+1} \mathbf{H}_{k+1}) \mathbf{P}_{k+1}^- \quad (20)$$

6. Observability Analysis

The new framework begs two different questions on observability: (i) Is there enough data available to derive/extract the POD modes for model order reduction? and (ii) can the reduced state, \mathbf{z} , be estimated using discrete point measurements of density along an orbit? The first question is easy to answer because unlike some previous works where the POD modes or EOFs are derived from discrete measurements of density along an orbit (e.g., Matsuo & Forbes, 2010), we use model simulation output that provides complete global spatial coverage to derive the POD modes. In addition, simulation output over a full solar cycle is used which ensures sufficient temporal coverage.

For linear time-invariant systems, such as the ROM formulation in equation (3), answer to the second question can be provided using the observability matrix

$$\mathcal{O}_k = \mathbf{H}_{r,k} \mathbf{A}_r^k \quad \Rightarrow \quad \mathcal{O} = \begin{bmatrix} \mathbf{H}_0 \\ \mathbf{H}_1 \mathbf{A} \\ \mathbf{H}_2 \mathbf{A}^2 \\ \vdots \end{bmatrix} \quad (21)$$

The matrix \mathcal{O} is populated at each time for the location at which the observation is made. The state \mathbf{z} is considered to be observable when the observability matrix is full rank or $\text{rank}(\mathcal{O}) = r$. In addition, the observability

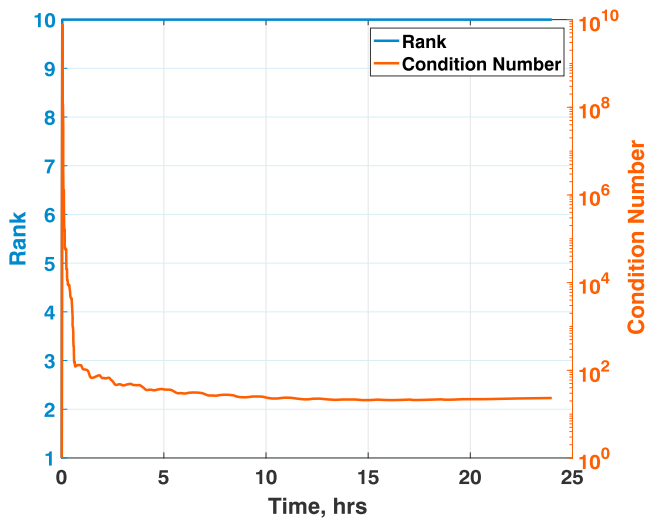


Figure 2. Rank and condition number of the observability matrix when assimilating CHALLENGING Minisatellite Payload measurements with TIE-GCM ROM on day 320 of year 2009.

matrix can artificially become full rank because of noise. Therefore, we also compute the condition number of \mathcal{O} to confirm that this is not the case. A relatively large condition number suggests that the observability matrix is not full rank due to noise. Figure 2 shows the rank and condition number for the real measurement demonstration case presented in this work assimilating a full days' worth of measurements along the CHAMP orbit for $r = 10$. The figure shows that the observability matrix becomes full rank very quickly. The condition number rises to very large values initially (large values correspond to ill-conditioned problem) and also falls back to a well-conditioned state quickly after full rank is achieved. This ill-conditioned period corresponds to the convergence dynamics of the Kalman filter.

7. Results and Discussion

We demonstrate the new framework by assimilating simulated and real measurements on day 320 of year 2009. We assimilate measurements along CHAMP orbit and validate with an independent set of measurements along the orbit of GOCE. The discrete time reduced-order dynamic and input matrices are converted to continuous time using the relation in equation (14). Since both the ingested and validation data sets have a time resolution of 10 s, we convert the dynamic and input matrices back to discrete time for a time step of 10 s.

7.1. Simulated Measurements

The simulated case uses MSIS model output along CHAMP and GOCE orbits on day 320 of year 2009. The CHAMP and GOCE MSIS densities are intercalibrated by scaling CHAMP densities using a daily value of 1.21. For the simulated case, we assume and apply the uncertainties associated with the real measurements to the simulated CHAMP and GOCE MSIS densities. The authors want to point out that the root-mean-square (rms) of uncertainties provided with the GOCE data set was on the order of 1%, which is too small even for the best drag coefficient and gas surface interaction models (Mehta, Walker, McLaughlin, & Koller, 2014). Therefore, we multiply the uncertainty by a factor of 5 to bring it to more reasonable values. Another major advantage of the new framework is that the ROM can be initialized using output from any model. Therefore,

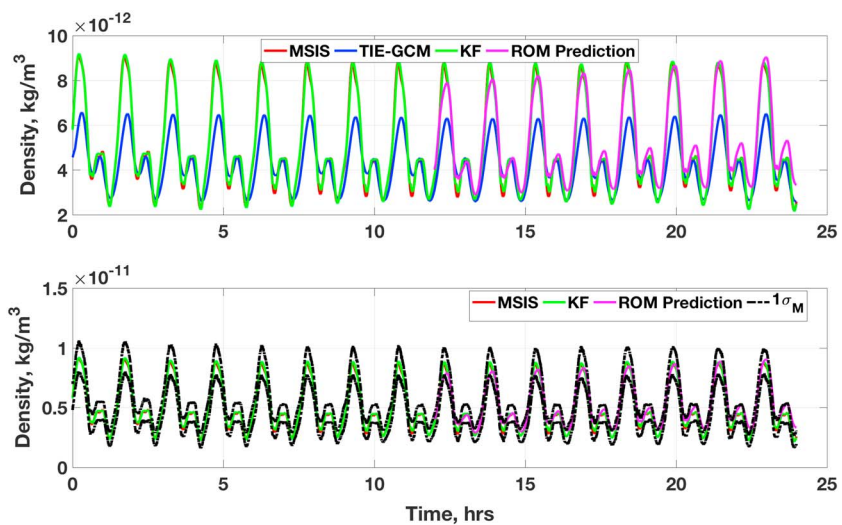


Figure 3. (top) Red: MSIS simulated measurements along CHAMP orbit on day 320 for year 2009. Blue: TIE-GCM densities along CHAMP orbit. Green: KF assimilated ROM density. Magenta: Prediction with ROM after 12 hrs of data assimilation. (bottom) Simulated MSIS (red), KF estimated (green), and ROM-predicted (magenta) densities with KF estimated 1σ uncertainties along CHAMP orbit. MSIS = Mass Spectrometer and Incoherent Scatter; TIE-GCM = Thermosphere-Ionosphere-Electrodynamics General Circulation Model; KF = Kalman filter; ROM = reduced-order model; CHAMP = CHALLENGING Minisatellite Payload.

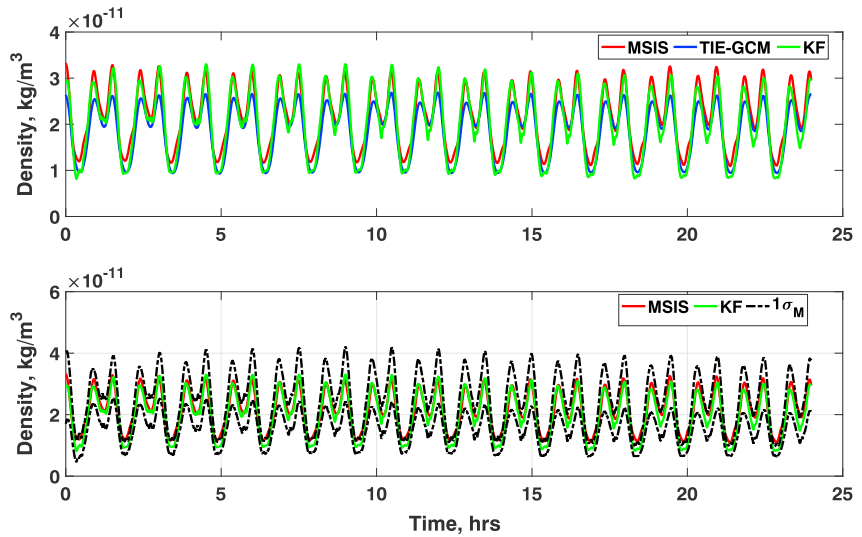


Figure 4. (top) Validation of the data assimilation process using MSIS simulated independent measurements (in red) along GOCE orbit on day 320 of year 2009. Blue: TIE-GCM densities along GOCE orbit. Green: KF assimilated ROM density. (bottom) Simulated MSIS- (red) and KF estimated (green) densities with KF estimated 1σ uncertainties along GOCE orbit. MSIS = Mass Spectrometer and Incoherent Scatter; TIE-GCM = Thermosphere-Ionosphere-Electrodynamics General Circulation Model; KF = Kalman filter; GOCE = Gravity Field and Steady-State Ocean Circulation Explorer.

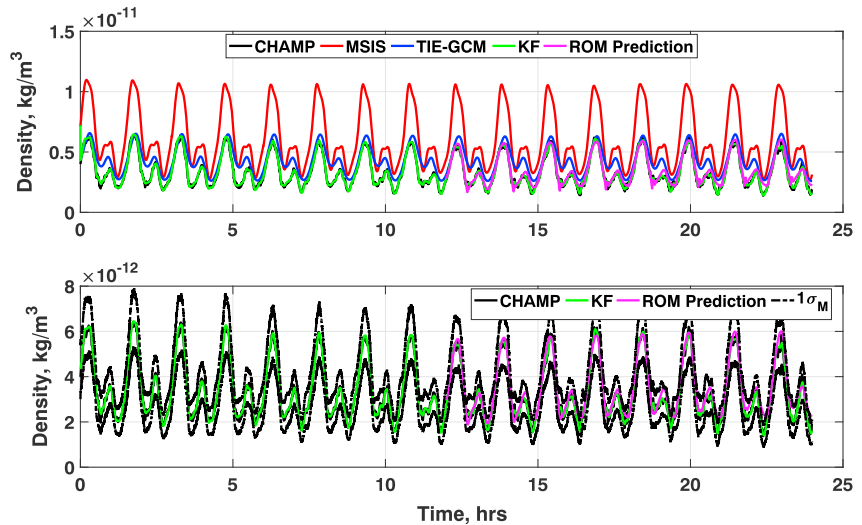


Figure 5. (top) Black: CHAMP accelerometer-derived density estimates. Red: MSIS model output along CHAMP orbit. Blue: TIE-GCM model output along CHAMP orbit. Green: CHAMP assimilated ROM densities on day 320 for year 2009. Magenta: prediction with ROM after 12 hrs of data assimilation. (bottom) CHAMP measurements (black), KF estimated (green), and ROM predicted (magenta) densities with KF estimated 1σ uncertainties along CHAMP orbit. MSIS = Mass Spectrometer and Incoherent Scatter; TIE-GCM = Thermosphere-Ionosphere-Electrodynamics General Circulation Model; KF = Kalman filter; ROM = reduced-order model; CHAMP = CHALLENGING Minisatellite Payload.

Table 1
RMS Difference for Real Measurements Case in Kilograms per Cubic Meters

Model → Satellite ↓	MSIS	TIE-GCM	Assimilated	
			MSIS initialized	TIE-GCM initialized
CHAMP	2.91e-12	1.02e-12	1.34e-13	1.30e-13
GOCE	7.24e-12	4.62e-12	2.18e-12	2.05e-12

Note. RMS = Root-Mean-Square; MSIS = Mass Spectrometer and Incoherent Scatter; TIE-GCM = Thermosphere-Ionosphere-Electrodynamics General Circulation Model; CHAMP = CHALLENGING Minisatellite Payload. GOCE = Gravity Field and Steady-State Ocean Circulation Explorer.

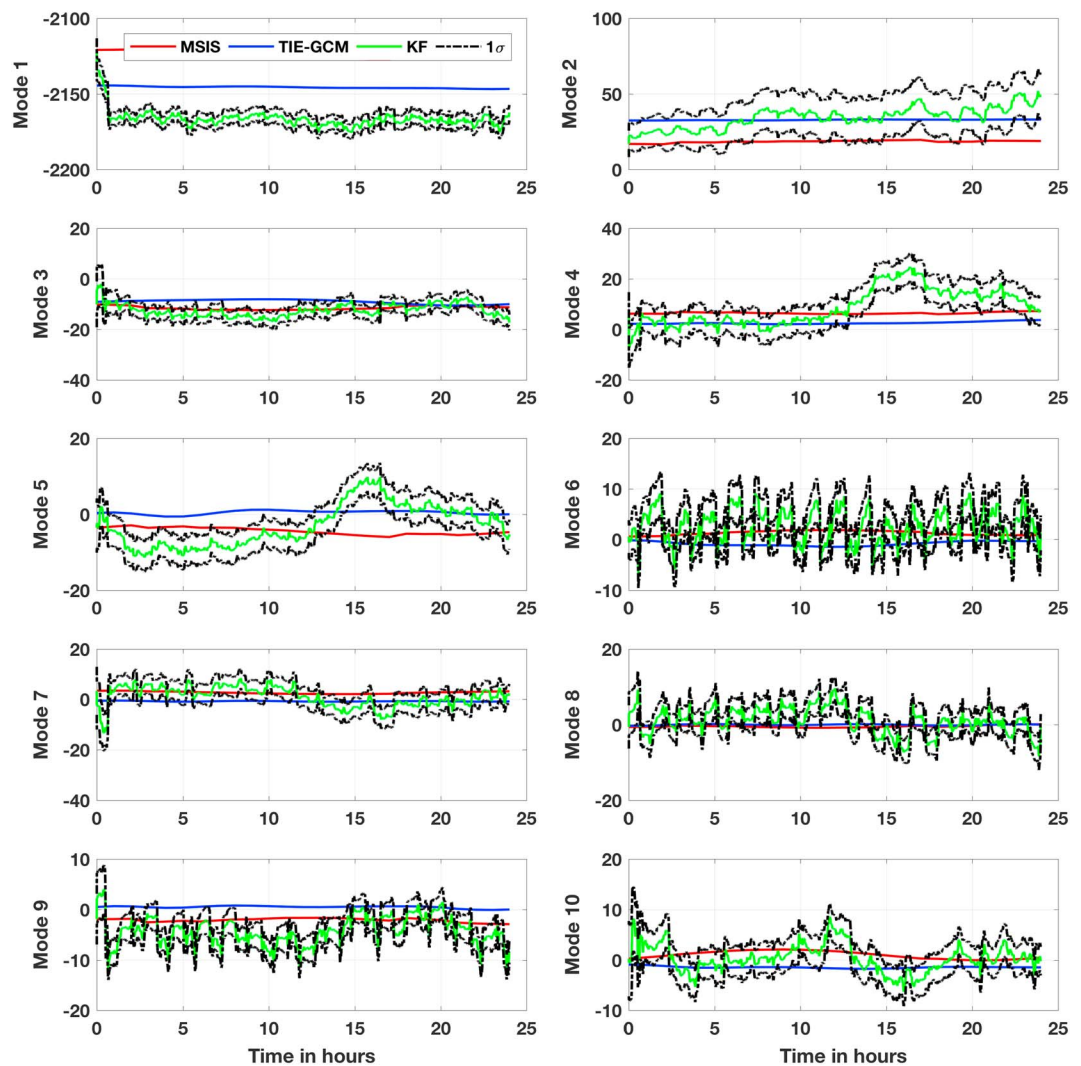


Figure 6. Red: POD coefficients for the first 10 modes computed by projecting MSIS simulation output onto the POD modes \mathbf{U}_j on day 320 of year 2009. Blue: POD coefficients for TIE-GCM. Green: KF estimated reduced-order state \mathbf{z} with data assimilation. Black: KF estimated 1σ uncertainty for the reduced-order state. MSIS = Mass Spectrometer and Incoherent Scatter; TIE-GCM = Thermosphere-Ionosphere-Electrodynamics General Circulation Model; KF = Kalman filter; POD = Proper Orthogonal Decomposition.

TIE-GCM simulations would not be required in case of an interruption in operations. The model can easily be reinitialized using output from empirical models. For demonstration with simulated measurements, the filter is initialized with TIE-GCM simulation output. The global density (full state) from TIE-GCM is used to compute the reduced state as $\mathbf{z}_0 = \mathbf{U}\mathbf{x}_0$.

Several different combinations of $[\hat{r}, r]$ were attempted with the combination $[10, 10]$ providing the best performance. This combination is a trade-off between accuracy and overfitting the measurements. Because MSIS is an averaged representation of the variations, a few modes (r) are enough to capture the dominant variations. Figure 3 shows the effectiveness of the data assimilation process through the new framework. The top panel shows the MSIS density along the CHAMP orbit (simulated measurements) in red, TIE-GCM densities along CHAMP orbit in blue, and the assimilated densities in green. We run an additional ensemble that sees data assimilation for the first 12 hrs but is then allowed to evolve under the dynamics captured by the ROM. This prediction is shown in magenta. It is observed that the approach tracks the simulated measurements very well and possesses very good potential for providing accurate forecasts. The forecast is expected to accumulate errors faster in time because of the low truncation order for both \hat{r} and r needed to avoid overfitting in this particular case (Mehta, Linares, and Sutton, 2018). The assimilation process in this case is mostly correcting

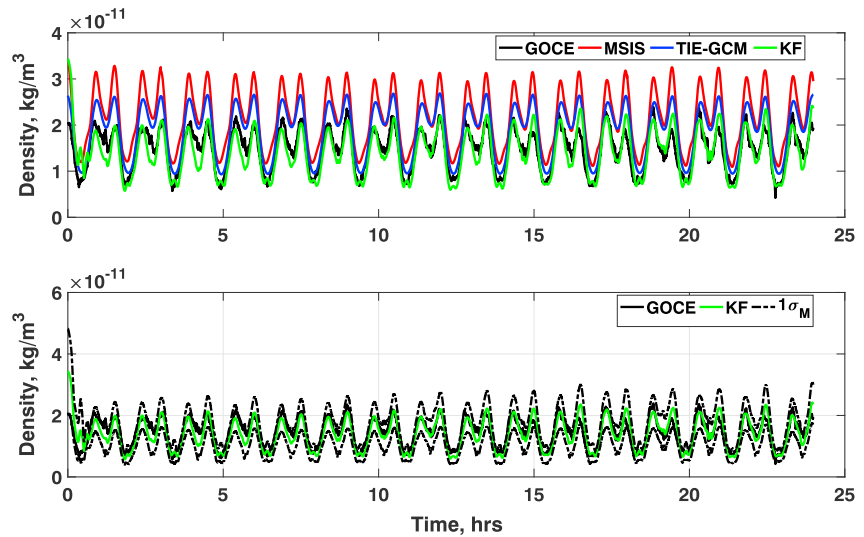


Figure 7. (top) Validation of CHALLENGING Minisatellite Payload data assimilation using independent measurements along GOCE orbit on day 320 of year 2009. Black: GOCE measurements. Red: MSIS output. Blue: TIE-GCM output. Green: KF estimates densities along GOCE orbit. (bottom) GOCE measurements (black) and KF estimated density and 1σ uncertainty along GOCE orbit. GOCE = Gravity Field and Steady-State Ocean Circulation Explorer; MSIS = Mass Spectrometer and Incoherent Scatter; TIE-GCM = Thermosphere-Ionosphere-Electrodynamics General Circulation Model; KF = Kalman filter.

for the difference in the day and night density magnitudes. It seems that MSIS overpredicts daytime densities, and since the model evolves through TIE-GCM dynamics, the prediction (magenta) attempts to match the magnitude variations but falls short. The bottom panel shows the simulated MSIS measurements (red) and the estimated (green) and predicted (magenta) densities with 1σ covariance bounds estimated as part of the data assimilation. The uncertainty bounds are computed by projecting the state covariance of equation (20) onto the measurement space

$$\mathbf{P}_k^{yy} = (\mathbf{H}_k \mathbf{P}_k \mathbf{H}_k^T + \mathbf{R}_k)^{0.5} \quad (22)$$

As seen, the measured (simulated) and predicted densities lie within the estimated 1σ uncertainty bounds. The full day pre-assimilation rms difference between TIE-GCM and MSIS (simulated measurements) densities along CHAMP orbit is $1.269\text{e}-12 \text{ kg/m}^3$, while post-assimilation the rms difference is $1.139\text{e}-13 \text{ kg/m}^3$.

Figure 4 shows the validation of the assimilation process using an independent set of simulated measurements (MSIS) along the GOCE orbit. The validation confirms that the reduced state, which provides global calibration, can be estimated using discrete measurements along a single orbit. The ROM is tuned with simulated MSIS density along the CHAMP orbit, with the corrected state accurately predicting the simulated MSIS density along GOCE orbit. Results show that the approach can self-consistently calibrate the model while preserving the underlying dynamics. The bottom panel shows that the simulated GOCE measurements lie within the estimated 1σ bounds. The pre-assimilation rms difference between TIE-GCM and MSIS (simulated measurements) densities along GOCE orbit is $3.078\text{e}-12 \text{ kg/m}^3$, while post-assimilation the rms difference is $2.137\text{e}-12 \text{ kg/m}^3$.

7.2. Real Measurements

The real data demonstration uses CHAMP (Mehta et al., 2017) and GOCE (Doornbos et al., 2014) accelerometer-derived densities on day 320 of year 2009. The CHAMP and GOCE densities are intercalibrated by scaling CHAMP densities using a daily value of 1.35. The uncertainties for GOCE are again scaled by a factor of 5 as discussed previously. Two different assimilation cycles are performed, one initialized with MSIS while the other initialized with TIE-GCM. Again, several different combinations of $[\bar{r}, r]$ are attempted with $[20, 10]$ providing the best results.

Figure 5 shows the assimilation results for the filter initialized with MSIS. Note: All the results shown in Figures 5 through 10 correspond to the case where the ROM is initialized with MSIS. Figures for TIE-GCM initialization are not shown to save on space. The top panel shows the CHAMP measurements in black, MSIS in red,

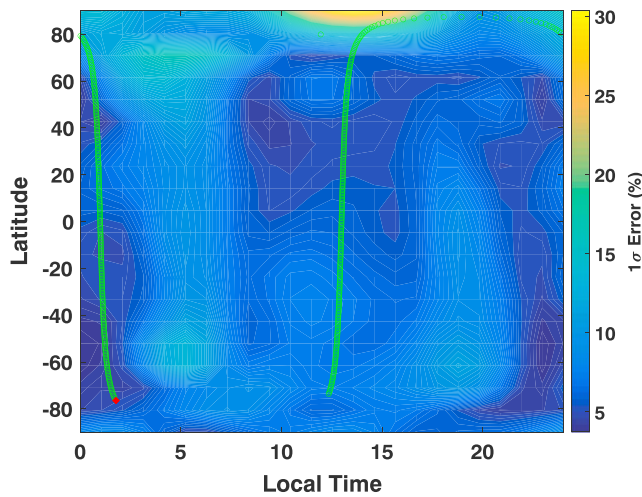


Figure 8. 1σ error prediction at mean CHAMP altitude after assimilation of all CHAMP data on day 320 of year 2009. Red: Satellite location at the current time. Green: back propagated CHAMP orbit from current location. CHAMP = CHALLENGING Minisatellite Payload.

TIE-GCM in blue, and the assimilated densities in green. The additional prediction ensemble is shown in magenta. Just as in the simulated case, the approach not only tracks the measurements very well but exhibits very good potential for providing accurate forecasts. In this case, the approach corrects for the both day-night magnitude difference and for the absolute scale biases, which represents the major component of the errors due to drag. The bottom panel shows the measurements (black), and the estimated (green) and the predicted (magenta) densities with 1σ covariance bounds estimated as part of the data assimilation. The uncertainty bounds are again computed by projecting the state covariance onto the measurement space. As seen, the measurements, and the estimated and predicted densities lie within the estimated 1σ uncertainties bounds. The pre-assimilation and post-assimilation rms difference values are given in Table 1.

Figure 6 shows the estimated reduced-order state and uncertainty with data assimilation. As previously discussed, the reduced state represents the POD coefficients for the first r modes used for order reduction. We also show the POD coefficients for MSIS and TIE-GCM obtained by projecting the simulation output for the day onto the POD modes. The first two modes correspond to absolute scale correction (scaling with solar activity), while others seem to represent variations on the different timescales.

Figure 7 shows the validation of the data assimilation using an independent data set of GOCE accelerometer-derived mass density. The validation again confirms that the reduced state, which provides global calibration, can be estimated using discrete measurements along a single orbit. The ROM is tuned with CHAMP densities, with the corrected state accurately predicting the density along GOCE orbit. Results show that the approach can self-consistently calibrate the model while preserving the underlying dynamics. The bottom panel shows that the GOCE measurements lie within the estimated 1σ bounds about the estimated density. The pre-assimilation and post-assimilation rms difference values are again provided in Table 1.

Table 1 also show the rms difference values for the real measurements case with initialization using TIE-GCM. The results, as anticipated, are very similar with TIE-GCM initialization slightly outperforming the initialization with MSIS. If the user prefers to initialize with TIE-GCM, a POD representation of the TIE-GCM simulation output using some form of regression can be used. Again, the TIE-GCM initialized results are not shown to save on space.

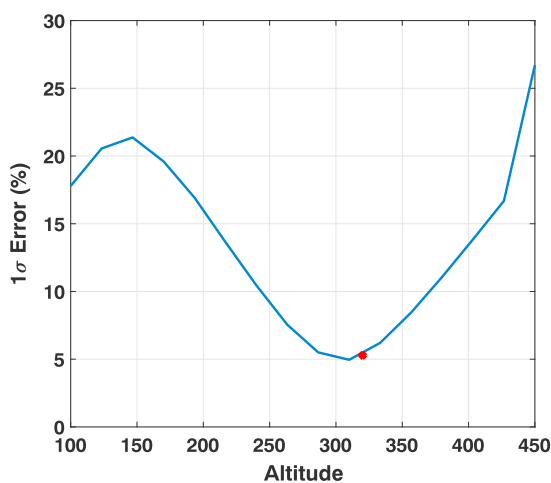


Figure 9. 1σ error prediction as a function of altitude after assimilation of all CHALLENGING Minisatellite Payload data on day 320 of year 2009. Red: Satellite location at the current time.

Figures 8 and 9 show the global estimated covariance as a projection away from the location of measurements. The green curve in Figure 8 represents CHAMP orbit path with the red point corresponding to the current location. The global uncertainty estimate is generated after all the data have been assimilated. The global field is generated using equation (22), but without the measurement error \mathbf{R} and with \mathbf{H} computed over the grid at the mean altitude of CHAMP. As seen, the uncertainty is reduced in the vicinity of the satellite path where the measurements are assimilated. The uncertainty is the largest at the pole because of the singularity constraint. The ROM captures the singularity constraint at the pole; however, assimilating inconsistent (densities derived using different methods) data can cause this constraint to not be satisfied, resulting in larger uncertainties close to the poles. It may be possible to force this constraint in the ROM framework and will be explored in future work. Figure 9 shows that the error is minimum at the altitude of CHAMP but increases moving away from the assimilated path. Even though ingesting data along an orbit path can provide global estimates using the new framework, the global errors, including close to the poles, can be further reduced with improved spatial and temporal coverage of measurements.

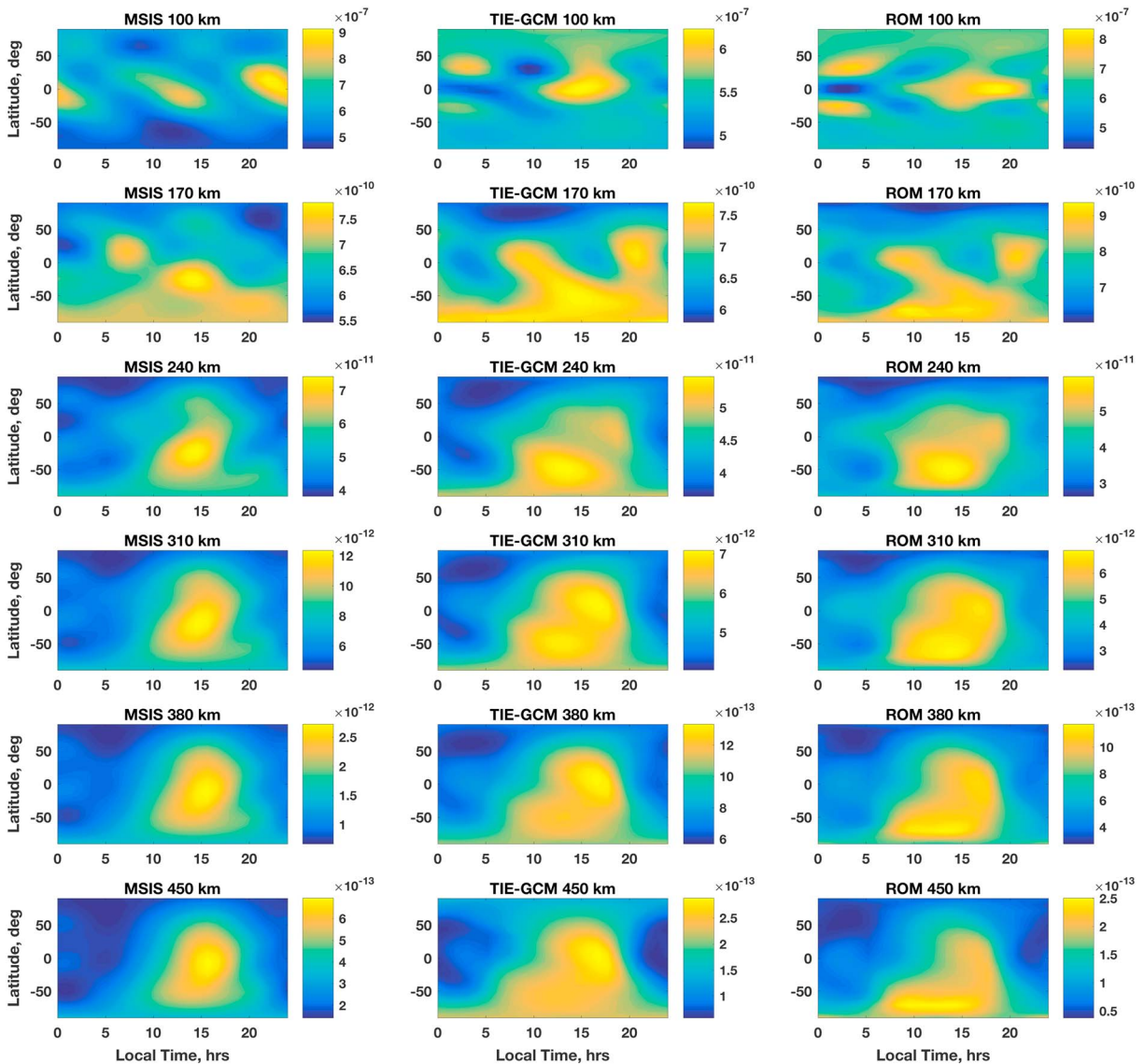


Figure 10. Comparison of mass density profiles at different altitudes from MSIS (left column) and TIE-GCM (middle column) against assimilated ROM mass density profiles at the same altitudes (right column) on day 320 of year 2009. MSIS = Mass Spectrometer and Incoherent Scatter; TIE-GCM = Thermosphere-Ionosphere-Electrodynamics General Circulation Model; ROM = reduced-order model.

Figure 10 shows the comparison of MSIS and TIE-GCM profiles against the ROM assimilated profiles at a series of altitudes. As seen, except for the profile at 100 km, the MSIS and assimilated ROM profiles show similar distributions. The difference at 100 km is due to the lower boundary effects. TIE-GCM and ROM have similar profiles at the lower boundary as expected. The absolute scale of the assimilated densities suggests that MSIS overpredicts the mass density across (almost) all altitudes during periods of low solar activity. While this is not a new revelation, the new framework effectively calibrates existing physical models by adjusting the absolute scale, which is a major driver of orbit prediction errors. Results also show that TIE-GCM slightly underpredicts mass density below about 250 km (GOCE altitude) on the day while overpredicting at higher altitudes.

8. Conclusions

This paper has demonstrated a new, transformative framework for data assimilation and calibration of physical IT models. A robust yet simple and effective approach for data assimilation has thus far eluded the community. The new framework has two major components: (i) Model order reduction for a quasi-physical linear

representation of the dynamics, and (ii) calibration of the ROM through data assimilation using a Kalman filter. Development of a ROM was discussed in a previous paper. This paper demonstrates the second component.

The new framework combines the best of both empirical and physical models. The ROM reduces the cost of model evaluation to the level of empirical models while inherently providing forecast/predictive capabilities. Unlike large-scale physical models, the ROM formulation allows rapid modifications in the time step of model evaluation or simulation with a negligible increase in the computational cost. This allows the model to be easily projected to the time of next measurement. The ROM formulation also allows large ensemble runs of the models for improved characterization and quantification of forecast uncertainty, a crucial requirement for accurate computation of collision probabilities.

Data assimilation using the new framework also carries several advantages. The data assimilation process estimates a reduced state that represents model parameters. Therefore, the data assimilation self-consistently brings the model to agreement with measurements without modifying the model dynamics. Also, estimating model parameters rather than the input(s)/driver(s) allows the model to be calibrated. The calibration avoids degradation of model performance in the absence of measurement data. The authors note that because the dynamics embedded in the ROM are derived from the TIE-GCM, the ROM carries the limitations of the TIE-GCM in terms of unmodeled dynamics as well as the use of proxy inputs such as $F_{10.7}$ and K_p . The assimilative formulation can statistically account for the unmodeled dynamics through the process noise; however, accurate forecasts will still depend on the accuracy of the space weather forecasts as well as the accuracy of its representation by the proxies.

The data assimilation cycle and prediction for a full day takes only a fraction of a second using minimal computational resources. Therefore, the framework can be readily incorporated into operations. The demonstration here is limited to non-storm time conditions. Future work will include development of ROMs that capture the nonlinear dynamics and demonstration of the data assimilation and prediction during storm time. The CHAMP and GOCE data used in this work are not considered operational data sets; therefore, future work will demonstrate the effectiveness of the framework with operational data sets such as Two-Line Element sets for well-behaved objects in LEO or other objects using recent advances for improved characterization of object parameters that affect drag (e.g., Mehta, Linares, & Walker, 2018) and computation of physical drag coefficients for complex objects (Mehta, Walker, Lawrence, et al., 2014).

Acknowledgments

The authors wish to acknowledge support of this work by the Air Force's Office of Scientific Research under contract FA9550-18-1-0149 issued by Erik Blasch. The authors wish to thank Humberto Godinez for insightful discussion on existing methods for data assimilation. The authors also wish to thank the anonymous reviewers for their helpful comments. No data were generated as part of this work. The CHAMP densities used in this work can be downloaded at <http://tinyurl.com/densitysets>. The GOCE densities data are provided by the European Space Agency and can be downloaded at <https://earth.esa.int/web/guest/missions/esa-operational-missions/goce/air-density-and-crosswind-data>. The TIE-GCM ROM used in this work can be downloaded at the University of Minnesota Digital Conservancy: <http://hdl.handle.net/11299/194705>.

References

- Barlier, F., Berger, C., Falin, J. L., Kockarts, G., & Thuillier, G. (1978). A thermospheric model based on satellite drag data. *Annales de Geophysique*, 34, 9–24.
- Bayes, T. (1763). "An essay towards solving a Problem in the Doctrine of Chances." Bayes's essay as published in the Philosophical Transactions of the Royal Society of London (Vol. 53, p. 370), on Google Books.
- Berger, C., Biancale, R., Barlier, F., & Ill, M. (1998). Improvement of the empirical thermospheric model DTM: DTM94—A comparative review of various temporal variations and prospects in space geodesy applications. *Journal of Geodesy*, 72, 161–178. <https://doi.org/10.1007/s001900050158>
- Bowman, B. R., Tobiska, W. K., Marcos, F. A., Huang, C. Y., Lin, C. S., & Burke, W. J. (2008). A new empirical thermospheric density model JB2008 using new solar and geomagnetic indices. In *AIAA/AAS Astrodynamics Specialist Conference and Exhibit*, Honolulu, Hawaii.
- Bowman, B. R., Tobiska, W. K., Marcos, F. A., & Valladares, C. (2008). The JB2006 empirical thermospheric density model. *Journal of Atmospheric and Solar-Terrestrial Physics*, 70, 774–793. <https://doi.org/10.1016/j.jastp.2007.10.002>
- Bruinsma, S. (2015). The DTM-2013 thermosphere model. *Journal of Space Weather and Space Climate*, 5(27), A1. <https://doi.org/10.1051/swsc/2015001>
- Bruinsma, S. L., Sanchez-Ortiz, N., Olmedo, E., & Guijarro, N. (2012). Evaluation of the DTM-2009 thermosphere model for benchmarking purposes. *Journal of Space Weather and Space Climate*, 2(27), A04. <https://doi.org/10.1051/swsc/2012005>
- Bruinsma, S., Thuillier, G., & Barlier, F. (2003). The DTM-2000 empirical thermosphere model with new data assimilation and constraints at lower boundary: Accuracy and properties. *Journal of Atmospheric and Solar-Terrestrial Physics*, 65, 1053–1070. [https://doi.org/10.1016/S1364-6826\(03\)00137-8](https://doi.org/10.1016/S1364-6826(03)00137-8)
- Codrescu, S. M., Codrescu, M. V., & Fedrizzi, M. (2018). An ensemble Kalman filter for the thermosphere-ionosphere. *Space Weather*, 16, 57–68. <https://doi.org/10.1002/2017SW001752>
- Codrescu, M. V., Fuller-Rowell, T. J., & Minter, C. F. (2004). An ensemble-type Kalman filter for neutral thermospheric composition during geomagnetic storms. *Space Weather*, 2, S11002. <https://doi.org/10.1029/2004SW000088>
- DeCarlo, R. A. (1989). *Linear systems: A state variable approach with numerical implementation*, Upper Saddle River, NJ, USA: Prentice-Hall, Inc.
- Doornbos, E., Bruinsma, S., Fritsche, B., Koppenwallner, G., Visser, P., Van Den IJssel, J., & de Teixeira de Encarnacao, J. (2014). GOCE+ Theme 3: Air density and wind retrieval using GOCE data (Final Report). Netherlands: TU Delft.
- Drinkwater, M. R., Floborghagen, R., Haagmans, R., Muzi, D., & Popescu, A. (2003). GOCE: ESA's first Earth explorer core mission. In G. Beutler, M. R. Drinkwater, R. Rummel, & R. von Steiger (Eds.), *Earth Gravity Field from Space—From Sensors to Earth Sciences, Space Sciences Series of ISSI* (Vol. 17, pp. 419–432). Dordrecht: Kluwer.
- Emmert, J. T., & Picone, J. M. (2010). Climatology of globally averaged thermospheric mass density. *Journal of Geophysical Research*, 115, A09326. <https://doi.org/10.1029/2010JA015298>

- Fuller-Rowell, T. J., Minter, C. F., & Codrescu, M. V. (2004). Data assimilation for neutral thermospheric species during geomagnetic storms. *Radio Science*, 39, RS1503. <https://doi.org/10.1029/2002RS002835>
- Godinez, H. C., Lawrence, E., Higdon, D., Ridley, A., Koller, J., & Klimenko, A. (2015). Specification of the ionosphere-thermosphere using the ensemble Kalman Filter. In S. Ravela & A. Sandu (Eds.), *Dynamic Data-Driven Environmental Systems Science* (pp. 274–283). Cambridge, United States: Springer International Publishing. https://doi.org/10.1007/978-3-319-25138-7_25
- Hedin, A. E. (1983). A revised thermospheric model based on mass spectrometer and incoherent scatter data MSIS-83. *Journal of Geophysical Research*, 88(A12), 10,170–10,188. <https://doi.org/10.1029/JA088iA12p10170>
- Hedin, A. E. (1987). MSIS-86 thermospheric model. *Journal of Geophysical Research*, 92(A5), 4649–4662. <https://doi.org/10.1029/JA092iA05p04649>
- Hedin, A. E., Reber, C. A., Newton, G. P., Spencer, N. W., Salah, J. E., Evans, J. V., et al. (1977). A global thermospheric model based on mass spectrometer and incoherent scatter data MSIS. I-N2 density and temperature. *Journal of Geophysical Research*, 82(16), 2139–2147. <https://doi.org/10.1029/JA082i016p02139>
- Jacchia, L. G. (1970). New static models of the thermosphere and exosphere with empirical temperature profiles. SAO Special Report, 313.
- Kalman, R. E. (1960). "A new approach to linear filtering and prediction problems". *Journal of Basic Engineering*, 82, 35. <https://doi.org/10.1115/1.3662552>
- Lumley, J. L. (1967). The structure of inhomogeneous turbulent flows. In A. M. Yaglam & V. I. Tatarsky (Eds.), *Proceedings of the international colloquium on the fine scale structure of the atmosphere and its influence on radio wave propagation*. Moscow, Nauka: Doklady Akademii Nauk SSSR.
- Matsuo, T., Fedrizzi, M., Fuller-Rowell, T. J., & Codrescu, M. V. (2012). Data assimilation of thermospheric mass density. *Space Weather*, 10, S05002. <https://doi.org/10.1029/2012SW000773>
- Matsuo, T., & Forbes, J. M. (2010). Principal modes of thermospheric density variability: Empirical orthogonal function analysis of CHAMP 2001–2008 data. *Journal of Geophysical Research*, 115, A07309. <https://doi.org/10.1029/2009JA015109>
- Matsuo, T., & Knipp, D. J. (2013). Thermospheric mass density specification: Synthesis of observations and models (AFRL Tech. Rep., DTIC ADA592729).
- Matsuo, T., Lee, I.-T., & Anderson, J. L. (2013). Thermospheric mass density specification using an ensemble Kalman Filter. *Journal of Geophysical Research: Space Physics*, 118, 1339–1350. <https://doi.org/10.1002/jgra.50162>
- Mehta, P. M., & Linares, R. (2017). A methodology for reduced order modeling and calibration of the upper atmosphere. *Space Weather*, 15, 1270–1287. <https://doi.org/10.1002/2017SW001642>
- Mehta, P. M., Linares, R. L., & Sutton, E. K. (2018). A quasi-physical dynamic reduced order model for thermospheric mass density via Hermitian Space Dynamic Model Decomposition. *Space Weather*, 16, 569–588. <https://doi.org/10.1029/2018SW001840>
- Mehta, P. M., Linares, R., & Sutton, E. K. (2018). A quasi-physical dynamic reduced order model for thermospheric mass density via Hermitian space-dynamic mode decomposition. *Space Weather*, 16, 569–588. <https://doi.org/10.1029/2018SW001840>
- Mehta, P. M., Walker, A. C., Lawrence, E., Linares, R. L., Higdon, D., & Koller, J. (2014). "Modeling satellite drag coefficients with response surfaces". *Advances in Space Research*, 54(8), 1590–1607. <https://doi.org/10.1016/j.asr.2014.06.033>
- Mehta, P. M., Walker, A. C., McLaughlin, C. A., & Koller, J. (2014). "Comparing physical drag coefficients computed using different gas-surface interaction models". *Journal of Spacecraft and Rockets*, 51(3), 873–883. <https://doi.org/10.2514/1.A32566>
- Mehta, P. M., Walker, A., Sutton, E., & Godinez, H. (2017). New density estimates derived using accelerometers on-board the CHAMP and GRACE satellites. *Space Weather*, 15, 558–576. <https://doi.org/10.1002/2016SW001562>
- Minter, C. F., Fuller-Rowell, T. J., & Codrescu, M. V. (2004). Estimating the state of the thermospheric composition using Kalman filtering. *Space Weather*, 2, S04002. <https://doi.org/10.1029/2003SW000006>
- Mockus, J. (1975). On Bayesian methods for seeking the extremum. In G. I. Marchuk (Ed.), *Optimization Techniques IFIP Technical Conference Novosibirsk, July 1-7, 1974. Optimization Techniques 1974. Lecture Notes in Computer Science* (Vol. 27). Heidelberg: Springer, Berlin. [https://doi.org/10.1007/3-540-07165-2\(55\)](https://doi.org/10.1007/3-540-07165-2(55))
- Morozov, A. V., Ridley, A. J., Bernstein, D. S., Collins, N., Hoar, T. J., & Anderson, J. L. (2013). Data assimilation and driver estimation for the Global Ionosphere-Thermosphere Model using the Ensemble Adjustment Kalman Filter. *Journal of Atmospheric and Solar-Terrestrial Physics*, 104, 126–136. <https://doi.org/10.1016/j.jastp.2013.08.016>
- Murray, S. A., Henley, E. M., Jackson, D. R., & Bruinsma, S. L. (2015). Assessing the performance of thermospheric modeling with data assimilation throughout solar cycles 23 and 24. *Space Weather*, 13, 220–232. <https://doi.org/10.1002/2015SW001163>
- Picone, J. M., Hedin, A. E., & Drob, D. P. (2002). NRLMSISE-00 empirical model of the atmosphere: Statistical comparisons and scientific issues. *Journal of Geophysical Research*, 107(A12), 1468. <https://doi.org/10.1029/2002JA009430>
- Proctor, J. L., Kutz, J. N., & Brunton, S. L. (2016). Dynamic mode decomposition with control. *SIAM Journal on Applied Dynamical Systems*, 15(1), 142–161.
- Qian, L., Burns, A. G., Emery, B. A., Foster, B., Lu, G., Maute, A., et al. (2014). The NCAR TIE-GCM: A community model of the coupled thermosphere/ionosphere system, *Modeling the ionosphere-thermosphere system, AGU Geophysical Monograph Series* (pp. 73–84). Washington: John Wiley & Sons.
- Radtke, J., Kebschull, C., & Stoll, E. (2017). Interactions of the space debris environment with mega constellations—Using the example of the OneWeb constellation. *Acta Astronautica*, 131, 55–68. <https://doi.org/10.1016/j.actaastro.2016.11.021>
- Reigber, C., Luhr, H., & Schwintzer, P. (2002). CHAMP mission status. *Advances in Space Research*, 30, 129–134. [https://doi.org/10.1016/S0273-1177\(02\)00276-4](https://doi.org/10.1016/S0273-1177(02)00276-4)
- Schmid, P. J. (2010). Dynamic mode decomposition of numerical and experimental data. *Journal of Fluid Mechanics*, 656, 5–28. <https://doi.org/10.1017/S0022112010001217>
- Shim, J. S., Kuznetsova, M., Rasttter, L., Bilitza, D., Butala, M., Codrescu, M., et al. (2014). Systematic evaluation of ionosphere/thermosphere (IT) models, *Modeling the ionosphere-thermosphere system* (pp. 145–160). Washington: John Wiley & Sons, Ltd. <https://doi.org/10.1002/9781118704417.ch13>
- Storz, M. F., Bowman, B. R., Branson, J. I., Casali, S. J., & Tobiska, W. K. (2005). High Accuracy Satellite Drag Model (HASDM). *Advances in Space Research*, 36(12), 2497–2505. <https://doi.org/10.1016/j.asr.2004.02.020>
- Sutton, E. K. (2018). A new method of physics-based data assimilation for the quiet and disturbed thermosphere. *Space Weather*, 16, 736–753. <https://doi.org/10.1002/2017SW001785>
- Tapley, B. D., Bettadpur, S., Watkins, M., & Reigber, C. (2004). The gravity recovery and climate experiment: Mission overview and early results. *Geophysical Research Letters*, 31, L09607. <https://doi.org/10.1029/2004GL019920>